JOURNAL OF GEOPHYSICAL RESEARCH, VOL. 100, NO. D11, PAGES 23,039–23,050, NOVEMBER 20, 1995

Airborne hydrogen peroxide measurements in supercooled clouds

Jefferson R. Snider and Todd Murphy

Department of Atmospheric Science, University of Wyoming, Laramie

Abstract. Airborne measurements of hydrogen peroxide and its partitioning between the aqueous and gas phases were conducted during studies of wintertime orographic clouds at temperatures ranging between -9° and -24°C. A subset of the derived values of the H_2O_2 Henry's law coefficient, based on measurement of gas-phase H_2O_2 and the physical properties of the cloud, were found to agree with laboratory measurements extrapolated to the cloud temperature. Disparities between the derived and temperature-extrapolated values were also observed, but this was attributed to overestimates of the in-cloud H_2O_2 mixing ratio that result from solute H_2O_2 volatilization on the reverse-flow air sample inlet during cloud droplet impaction and freezing. This hypothesis is supported by the fact that the derived Henry's law coefficients which exhibit agreement with the temperature-extrapolated values were conducted using a narrower inlet which intercepts less cloud water. Also discussed are vertical profiles of gaseous H_2O_2 within and above a cloud-capped boundary layer and in-cloud measurements which reveal that H_2O_2 scavenging by ice hydrometeors is minimal in comparison to uptake by an equivalent mass of liquid cloud droplets.

1. Introduction

Hydrogen peroxide (H_2O_2) is a gaseous trace constituent produced via reaction pathways initiated by the photolysis of ozone and terminated by recombination of the hydroperoxyl radical in either the gas phase or within liquid hydrometeors [*Gunz and Hoffmann*, 1990; *Faust et al.*, 1993]. *Penkett et al.* [1979] was the first to demonstrate that H_2O_2 serves as the primary oxidant in the production of sulfuric acid in cloud water with a *p*H of less than 4.5. This assertion is substantiated by two properties of the $H_2O/H_2O_2/SO_2$ system. First, H_2O_2 is highly soluble in liquid water; second, its rate of reaction with sulfur in the +4 oxidation state (S(IV)) is insensitive to cloud water *p*H. It is therefore important to know both how much tropospheric H_2O_2 there is relative to coreactant SO_2 and also the degree to which H_2O_2 is partitioned into both liquid water and ice hydrometeors.

The partitioning of H_2O_2 between cloud water and the gas phase is described by Henry's law which asserts a temperature-dependent proportionality between the concentration of dissolved H_2O_2 and the cloud interstitial gas partial pressure. Laboratory measurements of the Henry's law constant are limited to temperatures greater than 0°C [*Lind and Kok*, 1986; *Lind and Kok*, 1994]. Studies conducted using a counterflow virtual impactor deployed at a mountaintop research facility [*Noone et al.*, 1991] and using research aircraft [*Barth et al.*, 1989; *Macdonald et al.*, 1995] indicate that departures from the predictions of Henry's law can exist. The largest of these appear to be the result of the reaction of dissolved H_2O_2 with S(IV) either prior or subsequent to cloud water sample collection. *Macdonald et al.* [1995] conducted the only airborne measurements at temperatures colder than 0°C and in regions unaffected by reaction with S(IV). These workers found that in-cloud measurements of gaseous H_2O_2 were larger than predicted by Henry's law. Furthermore, the amount of H_2O_2 dissolved in the cloud water samples, collected as rime ice, was smaller than expected. On the basis of this work it is not clear if the observed departures from equilibrium result from overestimation of the Henry's law constant at supercooled temperatures or if they are an artifact of H_2O_2 loss due to volatilization during riming [*Snider et al.*, 1992a].

Here we report aircraft measurements of the gas/aqueous partitioning of H_2O_2 and derived values of the Henry's law constant. The latter quantity is also compared to temperature-extrapolated laboratory measurements. These studies were conducted in supercooled stratocumulus and altocumulus clouds (-9° to -24°C). Our approach is to compare the cloud interstitial values of H_2O_2 mixing ratio to the predictions of an equilibrium model. This technique sidesteps the possible problem of H_2O_2 destruction during droplet evaporation in a counterflow virtual impactor [*Noone et al.*, 1991] or via reaction during or subsequent to cloud water collection. In addition, we examine H_2O_2 partitioning in the presence of ice hydrometeors and present profiles of gaseous H_2O_2 through a cloud-capped continental boundary layer.

2. Experimental

A detailed description of the University of Wyoming King Air instrumentation is given by *Cooper et al.* [1984]. Instruments of greatest importance to this work are described below. Techniques used at the Elk Mountain Observatory (EMO) for the measurement of gaseous H_2O_2 and SO_2 and condensation nuclei (CN) are summarized by *Snider et al.* [1992a] and by *Politovich and Vali* [1983]. Techniques used to sample cloudy air at EMO using a reverse-flow inlet and the analyzer used for measurement of the oxides of nitrogen at the site are described below.

2.1. Airborne Measurements

The techniques of *Gordon and Marwitz* [1984] were used to process data from the PMS (Particle Measuring Systems, Inc.) 2DP and PMS-2DC optical array probes. One-second averages of crystal concentrations per unit size interval were used to calculate ice water content (IWC, gm/m^3) using power laws of the form $M = \alpha \cdot D^{\beta}$ which relate crystal mass (M, gm) to the 2DP and 2DC probe measurements of maximum particle dimension (D, μm). The coefficients α and β, which depend on

Paper number 95JD01942.
0148-0227/95/95JD-01942$05.00

ice crystal habit, were obtained from the studies of *Locatelli and Hobbs* [1974] and *Davis* [1974]. Variability in crystalline habit and statistical errors in α and β introduce factor of 2 or smaller uncertainties in the calculated values of IWC [*Detwiler et al.*, 1990].

Cloud liquid water content (LWC, cm^3m^{-3}) was measured using two different devices: the forward scattering spectrometer probe (FSSP) and a Commonwealth Scientific and Industrial Research Organization (CSIRO) probe. The CSIRO probe was not available during 1992, but for the studies conducted in 1991 we compare results obtained from both instruments. On the basis of this intercomparison we contend the negative bias associated with the FSSP LWC measurement is no larger than 20%. This value is utilized in our error analysis (see section 4.3.).

A hydroperoxide monitor based on the design of *Lazrus et al.* [1986] was used to assay H_2O_2 in air. The monitor was calibrated both before and usually subsequent to each flight using aqueous standards. We also conducted ground-based studies which demonstrated that there was negligible H_2O_2 loss in the sample inlet tubing. These studies, our modifications to the Lazrus et al. design, required for operation in a pressurized aircraft, and the algorithm used to process data from the hydroperoxide monitor, are described by *Murphy* [1993]. Uncertainties which propagate from errors in the parameters used in the data processing algorithm (i.e., flow rates (both stripping solution and air), detector sensitivity, signal offset, and H_2O_2 decomposition efficiency) were never larger than $\pm$ 0.1 parts per billion by volume (ppbv).

Signal outputs from the hydroperoxide monitor were corrected for time lags introduced by the delays due to flow in the sample inlet tubing ($\sim$3 s) and due to liquid analyte flow from the stripping coil to the fluorescence detector ($\sim$220 s). Values of the delay time were determined for each analysis interval by aligning the transition from clear-air to in-cloud conditions (indicated by measurements of droplet number concentration) to decreases in the measurements of H_2O_2 mixing ratio (χ, ppbv). The 1/e response time of the monitor (T_r, s) averaged 18.1 s (n=8, σ=5 s) and varied between 13.3 and 24.2 s. Sensitivity of the results to T_r were evaluated by employing the values 18.1 and 24.2 s in our analysis.

For the study intervals summarized in Table 3 the H_2O_2 decomposition efficiency ranged from 98 to 88% and the catalase-peroxidase/peroxidase signal ratio ranged between 0.16 and 0.40. Neither of these quantities were systematically different for the experiments conducted in 1991 and 1992. Our data processing algorithm is based on the assumption that the sampled organohydroperoxides do not react with catalase. A reasonable value of the organohydroperoxide/catalase to H_2O_2/catalase rate constant ratio (0.07, *Schonbaum and Chance*, [1976]) and the technique of *Claiborn and Aneja* [1991] was used to account for biases introduced by this assumption (see section 4.3.). The Claiborn and Aneja technique accounts for positive biases in the H_2O_2 measurement which increase with increasing H_2O_2 decomposition efficiency and with increasing values of the catalase-peroxidase/peroxidase signal ratio.

Air was sampled via the reverse-flow Teflon-lined inlet tubes shown in Figure 1. Both inlets protruded though the roof of the aircraft, but the 1991 inlet was located approximately 2 m forward of the location of the 1992 inlet. (The inlet mounting locations corresponded to positions B and C in Figure 1 of *Twohy and Rogers* [1993]). *Twohy and Rogers* [1993] observed depletions of LWC at the location of the 1992 inlet and generally smaller perturbations of the field at a sampling location (i.e., position A, their Figure 1) closer to the nose of the aircraft. Plausible effects of inlet location on our measurements of H_2O_2 are discussed in section 5.

Properties of the air sample inlets used in 1991 (outer diameter 9.6 mm) and 1992 (outer diameter 25.6 mm) are summarized in Table 1. For the calculations of droplet impaction efficiency we have idealized the inlet as a vertical cylinder. This idealization was validated by post-flight observations of ice deposits only on the forward-facing portion of the inlet. Compared to the 1991 inlet, predicted ice accretion rates on the inlet used in 1992 are $\sim$1.7 times larger. This is the result of two competing effects, both of which vary with increasing inlet diameter: (1) the decrease in droplet impaction efficiency (fourth column Table 1), and (2) the increase in droplet impaction area. Since H_2O_2 contained in cloud droplets is released during rime accretion [*Snider et al.*, 1992a], it is expected that the measurements of χ, particularly those conducted in 1992, were positively biased relative to that expected for equilibrium cloud conditions. The magnitude of this bias cannot be quantified, but differences between the extent of H_2O_2 partitioning derived from measure ments conducted in 1991 and 1992 are consistent with its presence. This inference is discussed in section 5.

During both field seasons, and for a range of droplet sizes consistent with that observed, values of the droplet Stokes number (*Stk*) are in excess of unity (see the fifth column of Table 1). *Vincent et al.* [1986] demonstrate that this is a necessary condition for inefficient droplet aspiration and it is therefore assumed that the sampled air stream is devoid of cloud droplets. This was substantiated by visual inspections of the inlet. We therefore base our analysis on the assumption that only cloud interstitial H_2O_2 is sampled by the reverse-flow inlet. Biases introduced by sampling the smallest cloud droplets have little or no effect on the results presented here [*Murphy*, 1993]. The model of *Lozowski et al.* [1983] was employed to calculate the ice substrate temperature; the largest value during these experiments was -4°C.

2.2. Surface Measurements

A device consisting of a small wind tunnel and a reverse-flow air sample inlet was used for sampling air at EMO. The studies of *Huang* [1994] demonstrate that there is little droplet aspiration by this device. The chemical sensors (H_2O_2, SO_2, and NO_y) were housed in the observatory, and air from the inlet was brought to them via a 9-mm ID Teflon tube. The CN were sampled via the inlet used by *Snider et al.* [1992a]. The oxides of nitrogen (NO_y) were measured at EMO using a Thermo Environmental Instrument Company model 42s analyzer. Calibration standards were prepared by dynamically diluting a bottled NO/N_2 standard with high purity air. The time response (1/e) of the analyzer is 30 s for a step input of 1 ppbv NO and the detection limit (defined at twice the standard deviation of the instrumental baseline) is 0.1 ppbv. The hydroperoxide monitor used at EMO was identical to the aircraft instrument.

2.3. Study Site, Cloud Environment, and Flight Patterns

Simultaneous airborne and ground-based measurements were made during these studies. The surface data were collected at Elk Mountain Observatory (EMO, 3.3 km above mean sea level (msl)), located near the top of Elk Mountain (41° 38' N, 106° 32' W) which defines the northern end of the Medicine Bow Range in southeastern Wyoming. In a manner similar to the studies reported by *Politovich and Vali* [1983], the measurements from EMO were used to augment the aircraft observations. The concurrent observations of the mixing ratios of H_2O_2, SO_2, and NO_y, and CN concentration are shown in Table 2. The tabulated values are averages from the 3- to 4-hour interval of the aircraft

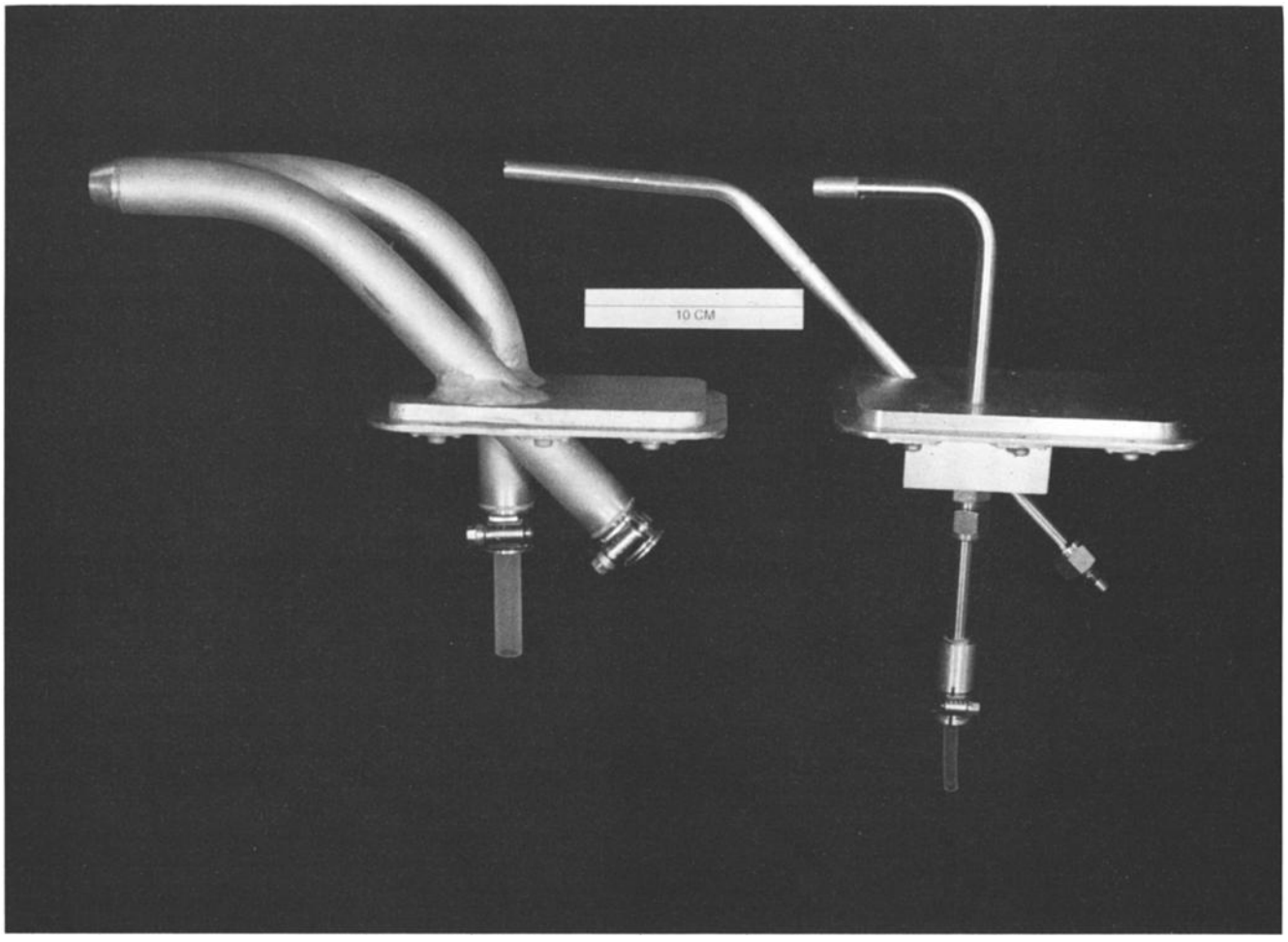

Figure 1. Reverse flow air inlets used on the UW King Air during measurements conducted in 1992 (left, rear) and in 1991 (right, front).

measurements. Companion studies of tracer SF_6 released within the boundary layer, by the aircraft, and detected at EMO [*Snider et al.*, 1992b] indicate boundary layer air was sampled at EMO. The measurements in Table 2 are thought to be representative of remote midcontinental conditions [*Ridley*, 1991; *Jaenicke*, 1993; *Hidy*, 1994] and demonstrate that the site is well removed from major pollution sources.

With the exception of the cloud pass from April 7, 1991, airborne measurements of in-cloud H_2O_2 partitioning were conducted in clouds that formed above either Elk Mountain or the Medicine Bow Range. The April 7, 1991 study was conducted in prefrontal stratocumulus clouds. Information pertinent to each of the nine cloud passes is given in Table 3. Data includes: cloud type and location, cloud pass averages of LWC and IWC, temperature, and measurements of the total H_2O_2 mixing ratio (X, ppbv). With the exception of the stratocumulus and altocumulus clouds observed on April 7, 1991 and January 16, 1992, respectively, the studied clouds could be classified as members of the "orographic" stratocumulus type characterized by Politovich and Vali. Cumuliform elements embedded within the larger stratiform cloud system were observed on all study days (except January 16, 1992) and cloud bases were always higher than the EMO. These characteristics should be contrasted with the smaller and more uniform Elk Mountain "cap" clouds that form at the top of the boundary layer and usually have bases below the mountain summit.

The flight pattern consisted of soundings, conducted over the North Platte river valley immediately upwind of Elk Mountain, and constant altitude cloud penetrations. Soundings were usually started at an altitude of 2.4 km msl (i.e., 760 mbar pressure altitude and approximately 300 m above the North Platte river valley) and were conducted at an ascent rate of less than 200 m/min. Observations from both the soundings and the cloud passes are discussed in sections 4, 4.1., and 4.2.

3. Calculations

The fractions, E, the scavenging efficiency for H_2O_2 derived using in-cloud and out-of-cloud gaseous H_2O_2 measurements, and E^*, the scavenging efficiency for H_2O_2 assuming Henry's law equilibrium, were both calculated at 1s intervals. E was calculated using

$$E = \frac{X - \chi}{X}. \quad (1)$$

Here X (ppbv) is a clear-air H_2O_2 measurement, χ is the cloud interstitial H_2O_2 measurement, and $(X - \chi)$ is the inferred

Table 1. Properties of the Reverse-Flow Inlets

Width W, μm	LWC L, cm^3m^{-3}	Droplet Diameter[1] D, μm	Droplet Impaction Efficiency[2] F	Droplet Stokes Number Stk
9.6	0.20	13.6	0.78	6.6
25.6	0.20	13.6	0.57	2.5
9.6	0.05	8.6	0.62	2.6
25.6	0.05	8.6	0.39	1.0

Width (W) is measured in millimeters, liquid water content (LWC) is measured in cubic centimeters per cubic meter, and droplet diameter (D) is measured in micrometers.

[1] Based on the assumption of a monodisperse population of cloud droplets and a droplet number concentration (150 cm^{-3}) consistent with cloud-pass-averaged FSSP measurements from this study [*Murphy*, 1993].

[2] From *Langmuir and Blodgett* [1946]), calculations shown here are for typical conditions: P = 600 mbar, T_a = -15°C, true air speed (U) = 100 m s^{-1}.

Table 2. Measurements from Elk Mountain Observatory

Date	H_2O_2, ppbv	SO_2, ppbv	NO_Y, ppbv	CN, cm^{-3}
March 20, 1991	0.15	<0.1	na[1]	200
March 22, 1991	0.25	<0.1	na	250
April 7, 1991	na	na	na	na
January 16, 1992	0.47	0.3	1.9	2700
February 13, 1992	0.33	0.2	2.0	500

H_2O_2, SO_2, and NO_Y are measured in parts per billion by volume. CN is measured in number per cubic centimeter.

[1] na = not available.

amount of cloud-water-dissolved H_2O_2. The assumption is that X, measured immediately prior to cloud entry, is representative of the total mixing ratio in-cloud (i.e., gaseous plus aqueous H_2O_2).

The equilibrium scavenging efficiency E^* is given by

$$E^* = \left(\frac{KLRT_aC_1}{C_2}\right) / \left(\frac{KLRT_aC_1}{C_2} + 1\right) \quad (2)$$

where K is the temperature-dependent Henry's law constant for H_2O_2 (M/atm), L is the LWC, T_a is the ambient temperature (K), R is the gas constant (8.314 J/(mol K)), and C_1 and C_2 are unit conversion factors equal to 10^{-3} L/cm^3 and 1.01325×10^5 Pa/atm, respectively. K was calculated using the expression of *Lind and Kok* [1994]:

$$K = \exp\left[\left(\frac{6638.}{T_a}\right) - 9.74\right]. \quad (3)$$

At temperatures less than 0°C, this formulation deviates less than 16% from predictions based on tabulated thermodynamic properties [*Wagman et al.*, 1982] and is also consistent with the recent work of *Staffelbach and Kok* [1993].

Because L and T_a were measured using instruments with higher frequency response characteristics than the hydroperoxide monitor, E^*, which is a function of both L and T_a (see (2)), was low-pass filtered using a recursive first-order Butterworth digital filter. The filter is expressed by

$$E^*_{filt,\,i} = E_i \quad (4)$$

for the first in-cloud measurement (i.e., i = 0), and for $i > 0$

$$E^*_{filt,\,i} = \frac{1-g(\nu_c)}{2} \cdot (E_i^* + E_{i-1}^*) + g(\nu_c) \cdot E^*_{filt,\,i-1} \quad (5)$$

where

$$g(\nu_c) = \exp\left[\frac{-2\pi\Delta t\nu_c}{\sqrt{10^{0.3}-1}}\right]. \quad (6)$$

In (6), Δt is the time interval between consecutive measurements (1 s), i is the index, and the cutoff frequency, ν_c, is related to T_r by

$$\nu_c = \frac{1}{2\pi T_r} \quad (7)$$

Using the filtered values of the equilibrium scavenging efficiency and assuming both that Henry's law holds and that X is representative of the total mixing ratio in-cloud, we derived the predicted in-cloud mixing ratio

$$\chi_p = X \cdot (1 - E^*_{filt}). \quad (8)$$

Values of the predicted Henry's law constant (K_p, M/atm) were also derived. From the previous two assumptions it follows from (1) that

$$E = \left(\frac{K_pLRT_aC_1}{C_2}\right) / \left(\frac{K_pLRT_aC_1}{C_2} + 1\right) \quad (9)$$

hence,

$$K_p = \frac{E \cdot \bar{K} \cdot (1 - E^*_{filt}))}{(1 - E) \cdot E^*_{filt}} \quad (10)$$

where $\bar{K}$ is the value of the Henry' law constant from (3) evaluated at the cloud-pass-averaged temperature.

The filter initial condition (cf.(4)) is equivalent to the assumption that the first value of χ_p, corresponding to the first second of the cloud pass, is equal to the first in-cloud measurement of χ. Because of this forced agreement, only subsequent values of χ and E, corresponding to measurements made beyond the edge of the cloud, are utilized to calculate the cloud-pass-averaged scavenging efficiency ratio, $\overline{E/E^*_{filt}}$, and the cloud-pass-averaged Henry's law constant, $\overline{K}_p$. If Henry's law holds, and our second assumption is valid, then $\overline{E/E^*_{filt}}$ is equal to unity and $\overline{K}_p$ is equal to $\overline{K}$. Scavenging efficiency ratios less than unity indicate an excess of cloud interstitial H_2O_2 (i.e., $\overline{K}_p < \overline{K}$), and ratios greater than unity indicate a deficit of cloud interstitial H_2O_2 (i.e., $\overline{K}_p > \overline{K}$).

Our calculations of the scavenging efficiency ratio and the Henry's law constant are based on two assumptions: (1) we assume that equilibrium between cloud interstitial and dissolved H_2O_2 is maintained, and (2) we assume that X is equivalent to the total hydrogen peroxide mixing ratio in-cloud,. The validity of these assumptions was tested by comparing values of the

Table 3. Analysis Intervals

Date	Analysis Interval, MST	Cloud Type/Location	Ice Crystal Habit[1]	Cloud-Pass Averages LWC[2], cm^3m^{-3}	Cloud-Pass Averages IWC[3], gm m^{-3}	Cloud-Pass Averages T_a, °C	X, ppbv Pre-cloud Entry	X, ppbv Sounding
March 20, 1991	1307:16 1308:27	Sc/Elk Mountain	P7b	0.19	0.03	-16	0.47	0.39
	1311:53 1313:53	Sc/Elk Mountain	P7b	0.21	0.18	-14	0.30	0.26
March 22, 1991	1722:09 1723:45	Sc/Elk Mountain	P1d	0.09	<0.01	-17	0.28	0.15 (in-cloud)
	1726:59 1727:45	Sc/Elk Mountain	P1d	0.05	<0.01	-18	0.22	0.23
April 7, 1991	0820:00 0822:26	Sc/50 km WNW from Elk Mountain	P7b	0.05	<0.01	-9	0.85	0.55 (in-cloud)
January 16, 1992	1724:11 1726:26	Ac/20 km ESE from Elk Mountain	C1g	0.07	<0.01	-23	1.03	na[4]
	1728:55 1730:13	Ac/20 km ESE from Elk Mountain	C1g	0.05	<0.01	-24	0.85	0.92
February 13, 1992	1211:54 1215:16	Sc/Elk Mountain	R4a	0.12	<0.01	-12	0.51	0.50
	1350:10 1352:17	Sc/25 km S from Elk Mountain	R4a	0.09	<0.01	-9	0.33	0.23 (in-cloud)

X is the total mixing ratio in parts per billion by volume. LWC is cloud liquid water content in cubic centimeters per cubic meter and IWC is calculated ice water content in gram per cubic meter.

1. Based on the Magono-Lee crystal classification scheme (see Pruppacher and Klett, 1984)

2. Cloud water content values are from the FSSP probe

3. Crystal mass (M, gm)-size (D, μm) relationships from Locatelli and Hobbs (1974) and Davis (1974) were used to calculate IWC. For hexagonal graupel (R4a) the relationship is $M = 0.089 \times 10^{-12} \cdot D^{2.9}$, for radiating assemblages of dendrites (P7b) $M = 74 \times 10^{-12} \cdot D^{1.9}$, for stellar crystals (P1d) $M = 4.1 \times 10^{-12} \cdot D^{1.9}$, and for solid thick plates (C1g) $M = 0.56 \times 10^{-12} \cdot D^{2.8}$.

4. na = not available

residence time of an air parcel within the cloud (τ_r) to the characteristic times for establishment of equilibrium between gaseous and aqueous H_2O_2 (i.e. τ_e, [*Jacob*, 1985]), for homogenization of entrained air parcels (i.e., τ_m), and for reaction of in-cloud SO_2 and H_2O_2 (τ_r). Estimates of these timescales are ranked in the following manner:

$$\tau_r\ (4000\text{-}3500\ s) > \tau_r\ (1500\text{-}500\ s) \geq \tau_m\ (1000\text{-}100\ s) > \tau_e\ (\approx 30\ s). \quad (11)$$

Values of τ_r, calculated using the SO_2 mixing ratio measurements in Table 2, are expected to be lower limit estimates, since *Faust et al.* [1993] have shown that H_2O_2 production via reaction in the aqueous phase is characterized by a time constant of $\sim 10^4$ s. The indicated range of τ_r corresponds to minimum and maximum values calculated as the ratio of cloud depth divided by a value of vertical velocity representative of the region of the cloud containing vertical velocities significantly greater than 0 m/s. Finally, the values of τ_m were calculated as

$$\tau_m = \left(\frac{\lambda_{max}^2}{\epsilon}\right)^{1/3} \quad (12)$$

where λ_{max} is the wavelength of the most energetic eddies in the inertial subrange (determined from plots of the variance spectra corresponding to in-cloud measurements of vertical velocity [*Politovich and Cooper*, 1988]), and ϵ is the eddy dissipation rate. Our analysis reveals that equilibrium between gaseous and aqueous H_2O_2 is expected since diffusion into the cloud droplets occurs on a timescale (30 s) substantially shorter than turbulent mixing (1000-100 s). Furthermore, depletion of H_2O_2 via reaction with SO_2 is not indicated, since the residence time of air parcels within the studied clouds (1500 - 500 s) is significantly shorter than τ_r.

4. Observations: Regions Containing Ice Only

Measurements of gaseous H_2O_2 during horizontal passes through regions containing no cloud water and IWC in excess of 0.01 gm/m^3, summarized in Table 4, were examined for changes due to either adsorption [*Conklin et al.*, 1993] or codeposition [*Jacob and Klockow*, 1993]. Data from April 7, 1991, shown in Figures 2a-2f, were obtained during a pass through a cloud region containing cloud droplets (i.e., prior to 0822:30 MST) and a subsequent pass through a liquid water depleted region containing enhanced concentrations of "precipitating ice" (larger than 1 mm). Measurements of pressure, temperature, and frost point temperature are shown in Figure 2a,

Table 4. Summary of Data From Cloud Regions Containing Only Ice

Date	Time, MST	Cloud-Pass Averages					
		T_a, °C	T_f[1], °C	N_{2DC}[2], L^{-1}	IWC[3], gm/m^3	Crystal Habit	H_2O_2 Depletion ?
March 20, 1991	1211:00 - 1212:20	-14	-20	9	0.02	R2b	NO
April 7, 1991	0828:20 - 0830:00	-7	-7	1	0.03	P7b	NO
February 13, 1992	1231:30 - 1236:00	-5	-7	1	0.03	R4a	NO

[1] Measurements of the water vapor saturation temperature obtained from the Cambridge Model 137C3 optical dew point hygrometer were assumed to be the frost point temperature (T_f)

[2] N_{2DC} is the crystal concentration from the PMS-2DC probe.

[3] Crystal mass (M, gm)-size (D, μm) relationships from *Locatelli and Hobbs* [1974] and *Davis* [1974] were used to calculate IWC . For hexagonal graupel (R4a) the relationship is $M = 0.089 \times 10^{-12} \cdot D^{2.9}$, for radiating assemblages of dendrites (P7b) $M = 74 \times 10^{-12} \cdot D^{1.9}$, and for densely rimed stellars (R2b) the relationship is $M = 1.9 \times 10^{-12} \cdot D^{2.3}$.

2DC probe crystal number concentration and concentrations of crystals larger than 1 mm (indicated by the open circles) detected by the 2DP probe are shown in Figure 2b, FSSP and CSIRO LWC (indicated by dots) and IWC are shown in Figure 2c, and the H_2O_2 mixing ratio (bold line) is plotted in Figure 2d. In the region containing only ice (i.e., subsequent to 0827:20 MST) variations in IWC were comparable to that observed in the liquid water cloud. Furthermore, particle growth by deposition was indicated by the measurements of T and T_f. However, a depletion of H_2O_2 was not observed. Data from the other two clouds summarized in Table 4 yielded the same result: uptake of H_2O_2 by ice hydrometeors is not detectable. The generality of this conclusion is limited, however, since IWC is sensitive to the number concentration of super-millimetric particles, which are expected to fall several hundred meters from their point of origin to the level at which they are observed. Also, since there is variability in the values of χ observed in clear air, the conclusion does not exclude the possibility that a small fraction of the H_2O_2 entering the cloud is scavenged by ice hydrometeors.

4.1. Observations: Vertical Profiles

Results from 2 days (March 22, 1991 and February 13, 1992) were selected to illustrate typical soundings obtained upwind of the studied clouds. Vertical profiles of T_a and T_f, virtual potential temperature (θ_v) and potential equivalent temperature (θ_e), water vapor mixing ratio (r) and LWC, ice crystal concentrations from the PMS-2DC (all sizes) and the PMS-2DP probes (sizes larger than 1 mm), and χ are shown in Figures 3a-4e. The measurements from February 13, 1992 (Figures 4a-4e), were conducted within 20 km of Elk Mountain. The upwind edge of the cloud, extending vertically from 670 to 585 mbar, was penetrated during the ascent. The sounding from March 22, 1991 (Figures 3a-3e), was obtained further upwind of the orographic cloud, and therefore liquid water cloud was only intercepted at 590 and 570 mbar. Vertically uniform values of θ_v and r are seen below approximately 700 mbar in both soundings. However in contrast to Elk Mountain cap clouds [*Cooper and Vali*, 1981; *Politovich and Vali*, 1983] the boundary layer is not separated from the air aloft by a strong capping inversion. Rather, the transition between the top of the boundary layer (indicated by BT in the right-hand margin) and cloud base (indicated by CB) was characterized by much weaker static stability. Decreasing θ_e with altitude either in the transition layer (Figure 3b) or within the boundary layer (Figure 4b) is also

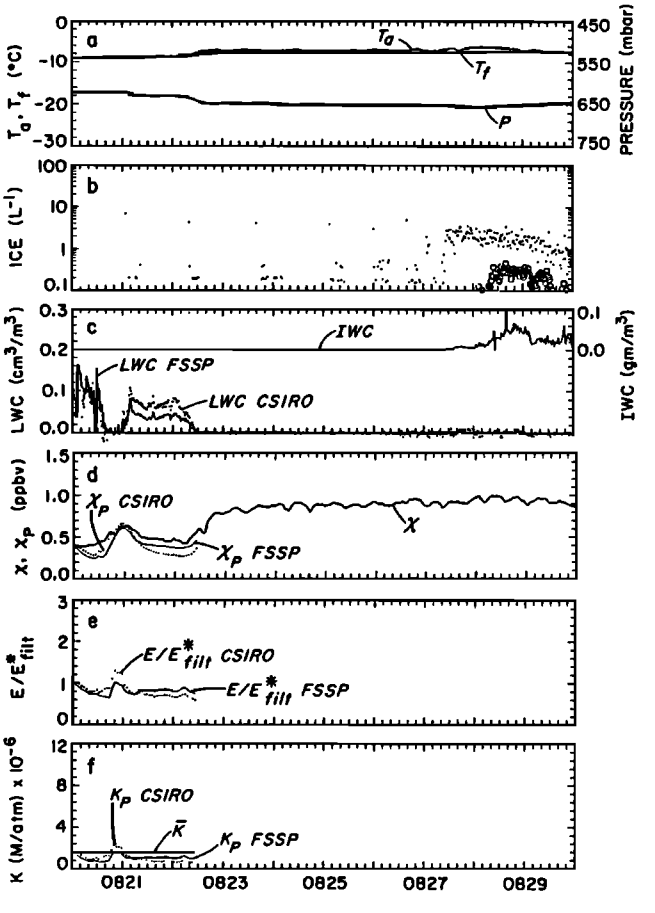

Figure 2. Aircraft measurements from April 7, 1991. (a) Ambient temperature (T_a), frost point temperature (T_f), and pressure (P); (b) Ice crystal concentration for particles larger than 1 mm (open circles), measured by the PMS-2DP probe, and ice crystal concentration measured by the PMS-2DC probe (dots); (c) FSSP LWC, CSIRO LWC, and IWC; (d) measurements of H_2O_2 mixing ratio (χ) and the predicted value (χ_p) derived using FSSP and CSIRO LWC measurements; (e) derived values of the scavenging efficiency ratio based on FSSP and CSIRO LWC; (f) predicted values of the Henry's law constant (K_p), derived using FSSP and CSIRO LWC measurements, and the value of $\bar{K}$ (3) corresponding to the cloud-pass-averaged temperature.

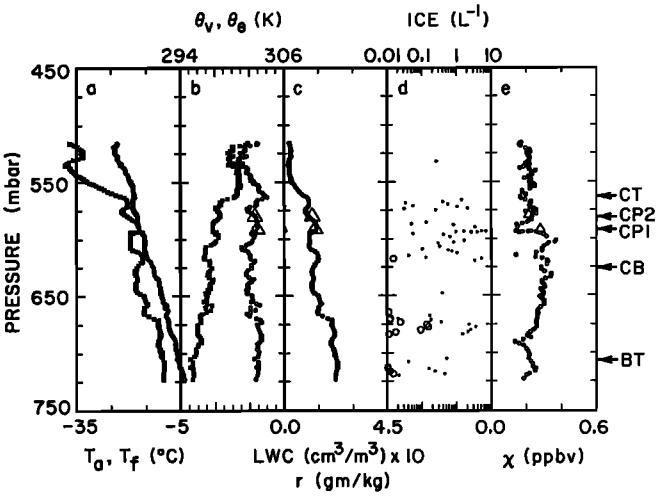

Figure 3. Nine second averages of data collected during the upwind sounding from March 22, 1991. (a) Ambient temperature (T_a), frost point temperature (T_f); (b) Potential equivalent temperature (θ_e) and virtual potential temperature (θ_v); (c) Water vapor mixing ratio (r, circles) and FSSP LWC (line); (d) Ice crystal concentration for particles larger than 1 mm (large open circles), measured by the PMS-2DP probe, and ice crystal concentration measured by the PMS-2DC probe (dots); (e) H_2O_2 mixing ratio (χ). Also plotted (open triangles) are the cloud-pass-averaged values of θ_e (Figure 3b) and r (Figure 3c), and the values of X (Figure 3e). Pressure altitudes corresponding to cloud top (CT), cloud pass 2 (CP2), cloud pass 1 (CP1), cloud base (CB), and the top of the boundary layer (BT) are indicated in the right-hand margin.

apparent. In both cases the vertical extent of the cloud was constrained by an absolutely stable inversion at ~575 mbar (indicated by CT). These observations suggest that the boundary layer and cloud layer are coupled via the orographically forced release of potential instability, a view consistent with visual observations of cumulus cloud elements embedded within the generally stratiform cloud layer. Similar to marine stratocumulus [*Nicholls*, 1984], the generation of potential instability appears to be driven by the vertical redistribution of the water substance. Visual observations of evaporating precipitation as well as the optical probe measurements showing super-millimetric particles at concentrations as large as 0.2 L^{-1} (see Figures 3d and 4d) support this contention.

Values of the pressure altitude corresponding to the cloud passes (indicated by CP1 and CP2) are shown in the right-hand margins of Figures 3 and 4. The comparison shown in Figures 3b and 3c, and 4b and 4c indicate a close match between sounding values of θ_e and r and those corresponding to the cloud passes (indicated by open triangles). This was the case for all of the studied clouds. With regard to θ_e this result is not surprising since the gradient $\partial\theta_e/\partial P$ is small everywhere below the inversion at cloud top. A more pronounced gradient in r, particularly between the top of the boundary layer and the altitude of the cloud pass, was always observed. This, combined with the agreement between cloud pass and sounding measurements seen in Figures 3b and 4b, supports the view that the cloud updrafts were composed of air parcels originating from within the cloud layer. Furthermore, good agreement between the pre-cloud values of X (indicated by open triangles in Figures 3e and 4e) and those measured during the sounding at the same pressure altitude as the cloud passes was also observed. This result is summarized in the eighth and final columns of Table 3.

The observations from both March 20, 1991, and April 7, 1991, were consistent with our interpretation of the cloud and boundary layer structure seen on both March 22, 1991, and February 13, 1992. Conditions were different on January 16, 1992, when a strong boundary layer capping inversion was observed, overlain by a deep layer, extending from 675 to 510 mbar, characterized by weak absolute stability. The altocumulus lenticular cloud monitored on this day was capped by an upper inversion based at 490 mbar.

The measurements of H_2O_2 shown in Figures 3e and 4e exhibit variability due to both the reversible uptake by cloud droplets and surface deposition. Deposition to the snow-covered surface, a process which is enhanced when temperatures approach 0°C [*Conklin et al.*, 1993], is indicated by the depressed values of χ seen below 725 mbar in Figure 4e. For the other cases, all with snow surface temperatures in excess of -5°C, nearly uniform profiles of χ were observed below 700 mbar. This difference is expected since systematically lower wind speeds, turbulence, and lower inferred rates of vertical mixing prevailed on February 13, 1992. The broad minimum in the measurements of H_2O_2 mixing ratio seen at ~610 mbar in Figure 4e is attributed to uptake by cloud droplets. The 0.4 ppbv decrease from cloud base to the region of maximum LWC is slightly less than that expected on the basis of Henry's law. Larger negative departures from the equilibrium prediction result if measurements from above 575 mbar are used in the comparison instead of the cloud base value. Data collected during some of the constant altitude cloud passes provide more convincing evidence for negative departures from Henry's law (i.e., an excess of cloud interstitial H_2O_2). These results are discussed in the following section. In contrast to the February 13, 1992 measurements, less vertical variability was seen in the H_2O_2 measurements from March 22, 1991 (Figure 3e). The depressed values of χ seen at ~590 mbar appear to be correlated with the observation of cloud water at this same altitude and are not inconsistent with uptake by the maximum values of LWC observed at this level (~0.03 cm^3m^{-3}).

4.2. Observations: Cloud Passes and H_2O_2 Partitioning

Cloud passes conducted on both March 22, 1991, and January 16, 1992, are shown in Figures 5a - 6f. Measurements are presented in the same manner as in Figures 2a-2d. Also shown

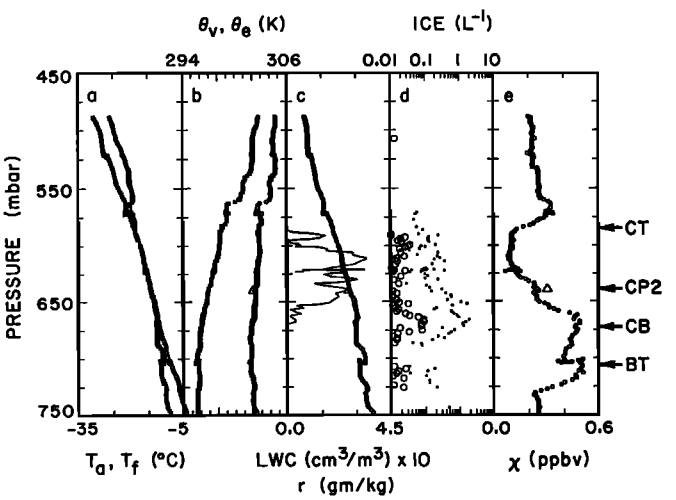

Figure 4. As in Figure 3 except for an upwind sounding conducted on February 13, 1992. Only the cloud-pass-averaged values of θ_e and r, and the value of X from the second cloud pass are indicated. At the time of first cloud pass (~1.5 hours earlier) significantly lower values of θ_e and r were observed within the cloud layer.

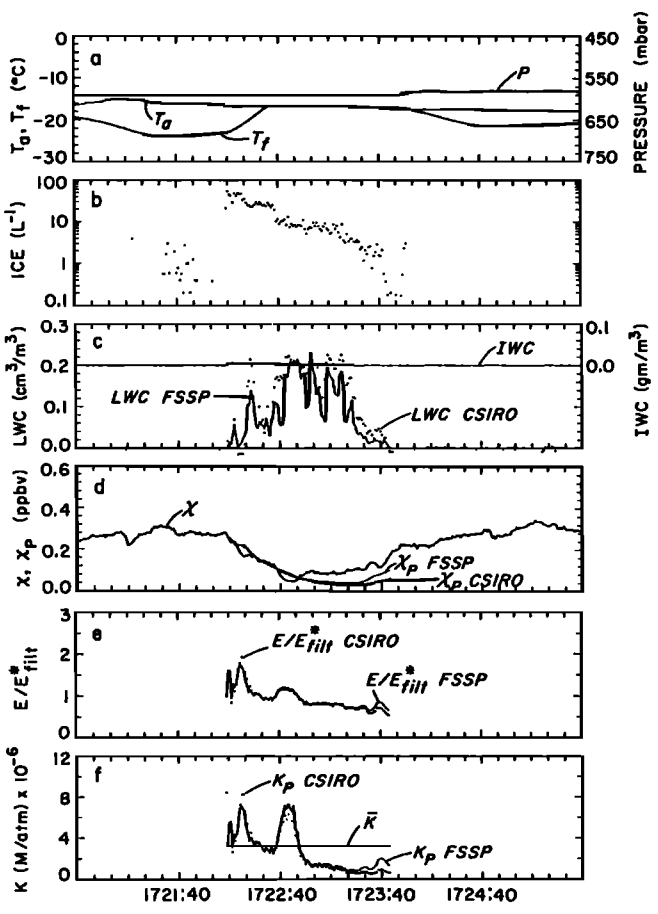

Figure 5. As in Figure 2 except for cloud pass 1 conducted on March 22, 1991.

are the values of χ_p (Figures 2d, 5d, and 6d), E/E^*_{filt} (Figures 2e, 5e, and 6e), and K_p (Figures 2f, 5f, and 6f). In Figures 2 and 5 these quantities were derived using both the CSIRO (dots) and FSSP water content values. During the flights conducted in 1992 the CSIRO probe was not operational so only the FSSP LWC measurements and quantities derived from it are shown in Figures 6c-6f. The results shown in Figures 2c and 5c demonstrate that there was good agreement (typically better than +20% or +0.05 cm^3m^{-3}) between the CSIRO and FSSP values of LWC. This was also the case for the other study conducted in 1991 (March 20, 1991). The cloud passes shown in Figures 5 and 6 were made while flying into the wind (east to west). These were followed by ascents to the altitude of a second cloud pass.

In contrast with the glaciated cloud observed on April 7, 1991 (Figure 2), and the mixed-phase cloud monitored on March 20, 1991 (Table 3), no particles larger than 1 mm were observed during the penetrations shown in Figures 5b and 6b, nor was the IWC larger than 0.01 gm/m^3 (Figures 5c and 6c). For the reasons discussed in section 4 it is unlikely that these particles perturbed the cloud interstitial values of χ.

Results of the H_2O_2 partitioning analysis are illustrated in the bottom three panels of Figures 2, 5, and 6. Here it is evident that the shape of the traces of χ and χ_p are comparable in all instances. Both quantities decrease with increasing LWC and increase at cloud exit. Negative departures from Henry's law equilibrium, indicated by values of χ larger than χ_p (Figures 2d, 5d, and 6d), scavenging efficiency ratios less than unity (Figures 2e, 5e, and 6e), K_p less than $\bar{K}$ (Figure 2f, 5f, and 6f), were observed during all cloud passes. Examples of this are most evident in Figures 6e where values of E/E^*_{filt} are uniformly less than 0.7. It is important to note that the difference χ - χ_p during this cloud pass, shown in Figure 6d, is substantially larger than both the measurement uncertainty and the variability of χ outside of the cloud.

Positive departure from Henry's law are evident during two intervals, centered at 1722:20 MST and at 1722:45 MST, in Figures 5d-5f. These events are associated with fluctuations in χ similar to that observed outside the cloud (at 1721:10 MST and 1724:50 MST) and the departures χ - χ_p seen in Figure 5d are comparable to the random error associated with the measurement (0.1 ppbv, see section 2.1.). Furthermore, the width of these features is shorter than the response time of the hydroperoxide monitor, and they do not correlate with variations in any of the cloud properties plotted in the top panels of Figure 5. For all of these reasons, and because the low frequency variations in both χ_p and χ are well correlated, we feel that the averages of the scavenging efficiency ratio and the Henry's law constant are the most reliable indicator of the extent of H_2O_2 partitioning. In the following section we examine how these averages are affected by measurement uncertainties.

4.3. Error Analysis

Errors in the cloud-pass averages $\overline{E/E^*_{filt}}$ and $\bar{K}_p$ result from uncertainties in the measurements of the physical and chemical properties of the observed clouds. *Murphy* [1993] examined the sensitivity of $\overline{E/E^*_{filt}}$ to perturbations in T_a, K, v_c, χ, LWC, and X and found that significant negative biases can result from

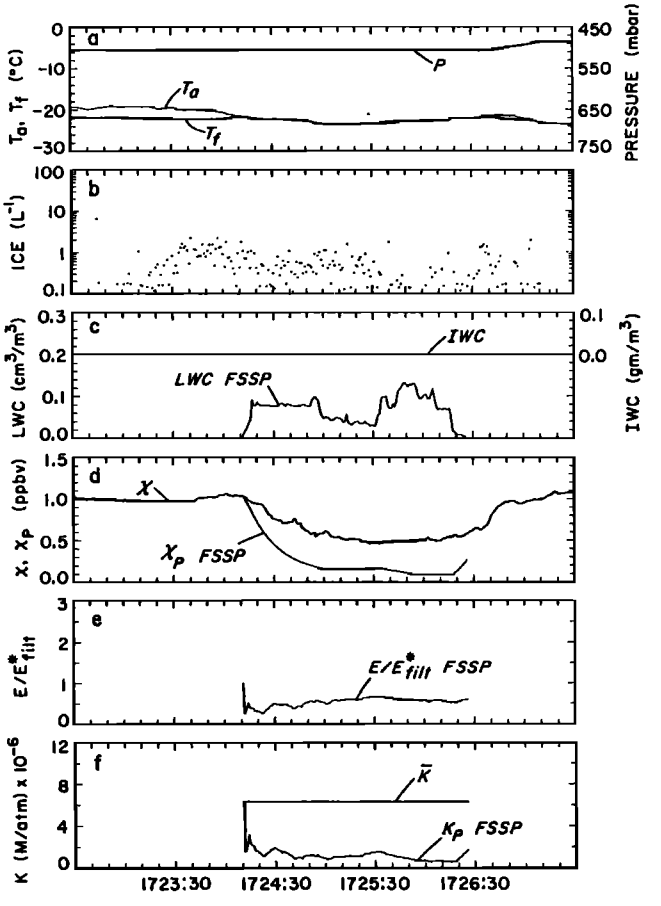

Figure 6. As in Figure 2 except for cloud pass 1 conducted on January 16, 1992. Note also that only FSSP LWC measurements are available on this day.

uncertainties in: (1) LWC, (2) total H_2O_2 mixing ratio (X), (3) cutoff frequency (ν_c), and (4) due to the organohydroperoxide/catalase reaction [*Claiborn and Aneja*, 1991]. We express the effect of these biases as a percentage change relative to the values of $\overline{E/E^*_{filt}}$ summarized in the second column of Table 5. Also shown in Table 5 are values of $\overline{E/E^*_{filt}}$ calculated using the CSIRO probe measurements of LWC, and the cloud-pass-averaged Henry's law constant ($\overline{K_p}$) based on both the FSSP and CSIRO probe measurements of LWC. The FSSP-based values of $\overline{E/E^*_{filt}}$ are larger, due to systematically smaller FSSP LWC, or they agree with the CSIRO-based values.

For our uncertainty analysis we utilized the FSSP LWC values and assumed that a -20% bias defines the minimum possible value for LWC. This assumption is consistent with the fact that the FSSP LWC values were typically smaller than that measured with the CSIRO probe (see Figures 2c and 5c). A -20% perturbation of the FSSP LWC increases $\overline{E/E^*_{filt}}$ by less than 9%. Biases in $\overline{E/E^*_{filt}}$ due to uncertainty in X result because we assume that the H_2O_2 mixing ratio measurements made immediately prior to cloud entry (see Table 3) are equal to the sum of interstitial and dissolved H_2O_2 within cloud. Measurements made in clear air below the cloud-capping inversion reveal that fluctuations in χ are as large as ±25%. The affect on $\overline{E/E^*_{filt}}$ of a +25% perturbation in X (only positive perturbations in X are considered since negative values of E result when X is decreased to less than the value of χ observed in cloud) is largest when $\overline{E/E^*_{filt}}$ is small and varies between +52% (cloud pass 1 conducted on February 13, 1992) and +6% (cloud pass 1 on March 22, 1991). Decreasing the cutoff frequency from 0.0088 Hz, corresponding to the average value of the response time T_r=18.1 s (see section 2.1. and (7)), to the smallest value observed (0.0066 Hz) perturbs $\overline{E/E^*_{filt}}$ by less than +13%. Finally, $\overline{E/E^*_{filt}}$ increases by less than +14% due to the reaction of organohydroperoxides. The combined effect of the measurement biases, shown in Figures 7a -7b, was evaluated using the perturbed values of FSSP LWC (-20%), X (+25%), ν_c (-25%), and in-cloud H_2O_2 mixing ratio. Biases in the latter quantity, resulting from the reaction of sampled organohydroperoxides with catalase, varied between +8 and +26%. It is evident that the upper limit estimates of $\overline{E/E^*_{filt}}$ are equal to or larger than unity for those experiments conducted in 1991. In contrast, all of the 1992 scavenging efficiency ratios are significantly smaller than unity, and similarly, all of the derived values of the Henry's law constant from 1992 are significantly smaller than extrapolations of the laboratory measurements. The latter results are shown in Figure 7b. A plausible explanation for the negative departures from Henry's law is discussed in the following section.

5. Discussion

Negative deviations from Henry's law equilibrium, indicated by values of $\overline{E/E^*_{filt}}$ less than unity in Figure 7a, were evident for all of the analyzed cloud passes. For the 1992 cases the disparity was found to be substantially larger than the upper limit estimates of the measurement biases. Here we investigate the possibility that H_2O_2 volatilization due to riming on the forward-facing surface of the air sample inlet is an important factor leading to this disparity. Our approach is to consider the sampled H_2O_2 as a mixture resulting from two sources: (1) air stripped of cloud water by impaction on the forward-facing surface of the sample inlet, and (2) unperturbed cloud-interstitial air. We indicate the relative amount of sources 1 and 2 by f_1 and f_2, respectively. The value of f_1 depends on the fraction of the LWC impacted on the sample inlet (F), the equilibrium scavenging efficiency for hydrogen peroxide (E^*_{filt}), the retention efficiency (Γ) for H_2O_2 (an upper limit value of 0.3 is assumed based on the work of *Snider et al.* [1992a]), and the observed values of χ and X. These dependencies are shown in (13).

$$f_1 = \frac{\chi - X(1 - E^*_{filt})}{XFE^*_{filt}(1 - \Gamma)} \quad (13)$$

Cloud pass averages of f_1 ranged between 0.1 and 0.4 for the 1991 analysis intervals and between 1.1 and 1.5 for the 1992 analysis intervals. Values of f_1 larger than unity are thought to indicate that Γ for these studies is smaller than that anticipated based on the work of *Snider et al.* [1992a], or that the sampled air is also influenced by riming on surfaces other than the forward-facing surface of the inlet. Observations of increasing LWC with distance from the roof of a King Air [*Twohy and Rogers*, 1993], especially at the sample inlet location used during our 1992 measurements, lend validity to the latter hypothesis. The fact that the 1991 values of f_1 are less than unity and small in comparison with the 1992 values seems sufficient to establish the point that the 1991 cloud passes were substantially less affected by H_2O_2 release during riming, a result consistent with the smaller cross-sectional area of the inlet and the more forward location of the 1991 inlet. As illustrated in Figure 7b, agreement between the Henry's law constants derived using data collected in 1991 and extrapolations of the laboratory measurements also supports this hypothesis.

Our assessment of the behavior of H_2O_2 in ice-only clouds appears to be consistent with the work of *Jacob and Klockow* [1993] who measured H_2O_2 incorporation into ice during H_2O_2/H_2O codeposition. For example, if the values of T_a, T_f, and IWC corresponding to the measurements conducted on April 7, 1991 (see Table 4), are used to predict H_2O_2 uptake by codeposition, we find that only 0.02 ppbv is sequestered. Note that this corresponds to only 2% of the amount observed in clear-air. The predicted depletion is therefore substantially smaller than the variability in H_2O_2 mixing ratio seen outside of cloud (see Figure 2d). Hence in comparison with partitioning

Table 5. Cloud-Pass-Averaged H_2O_2 Scavenging Efficiency Ratios and Henry's Law Constants

Date	FSSP $\overline{E/E^*_{filt}}$	CSIRO $\overline{E/E^*_{filt}}$	FSSP $\overline{K}_p$, M/atm	CSIRO $\overline{K}_p$, M/atm
March 20, 1991	0.82	0.79	2.0×10^6	1.9×10^6
	0.97	0.87	2.5×10^6	1.7×10^6
March 22, 1991	0.96	0.93	2.8×10^6	2.5×10^6
	0.92	0.79	3.4×10^6	2.3×10^6
April 7, 1991	0.82	0.82	1.0×10^6	1.0×10^6
January 16, 1992	0.54	na [1]	1.1×10^6	na
	0.41	na	1.3×10^6	na
February 13, 1992	0.40	na	0.32×10^6	na
	0.60	na	0.58×10^6	na

[1] na = not available

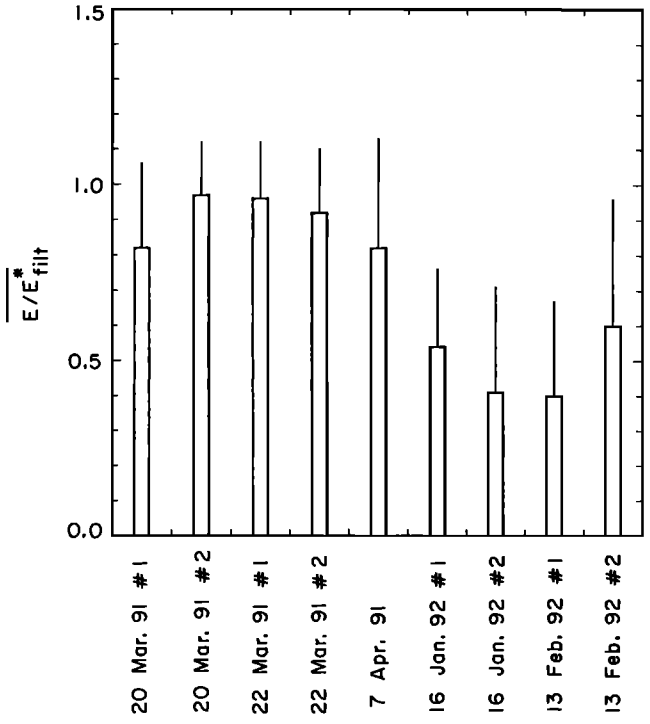

Figure 7a. Cloud-pass averaged H_2O_2 scavenging efficiency ratio for measurements conducted in 1991 and 1992. The upper limit error bars were calculated using the technique discussed in the text.

into an equal mass of condensed liquid water, H_2O_2 uptake via codeposition is expected to be at least an order of magnitude less efficient. Furthermore, in supercooled clouds containing graupel the removal of H_2O_2 is inhibited by the fact that a large fraction of solute H_2O_2 is volatilized during riming [*Snider et al.*, 1992a]. We note however that the work of *Jacob and Klockow* [1993] points to increasing H_2O_2 scavenging with IWC and therefore to the need for concurrent measurements of the amount present in the gas, liquid, and solid ice phases.

The cloud passes documented in Table 3 were characterized by mixing times (τ_m, see section 3) substantially larger than the time interval required for establishment of Henry's law equilibrium. However, in-cloud values of χ were always smaller than X and therefore our analysis of the characteristic times does not preclude the possibility of small negative deviations from Henry's law as a result of mixing. The magnitude of the deviation may also be enhanced if entrained air originates from cloud top where enhanced hydrogen peroxide mixing ratios have been documented [*Heikes et al.*, 1987; *Gallagher et al.* 1990]. Increases in H_2O_2 mixing ratio above cloud top were observed on both February 13, 1992 (Figure 4e), and on April 7, 1991. This phenomenon was not observed on March 22, 1991 (Figure 3e) or on the other study days. *Murphy* [1993] analyzed a cloud pass from April 7, 1991, which was associated with values of E/E^*_{filt} significantly smaller than unity and with values of eddy dissipation rate increasing to ~ 100 cm^2/s^3 in the regions of the cloud associated with the smallest value of E/E^*_{filt}. The observations of enhanced turbulence, elevated values of χ at cloud top, and depressed values of the scavenging ratio indicate that in some situations entrainment can influence the partitioning of H_2O_2. Values of eddy dissipation rate were generally lower than 30 cm^2/s^3 during all other cloud passes, and did not exhibit an inverse correlation with E/E^*_{filt}. For these reasons we believe that mixing is of secondary importance to airframe icing as a cause for the observed departures from Henry's law equilibrium.

6. Conclusions

We have presented measurements of gaseous H_2O_2 in both glaciated and mixed phase supercooled clouds. Substantial depletions of H_2O_2, evaluated as the difference between clear air and in-cloud measurements, were observed. This is attributed to the uptake of H_2O_2 by the cloud droplets, a process that can be described independently in terms of the Henry's law coefficient and the measured physical properties of the cloud. The derived properties E/E^*_{filt} and K_p, and the corresponding cloud-pass averages $\overline{E/E^*_{filt}}$ and $\overline{K}_p$, are predicated on the assumption that equilibrium between cloud interstitial and dissolved H_2O_2 is maintained. Since we show that uptake by ice hydrometeors is not appreciable, that in-cloud air parcel residence times are small relative to the time constant for reactive depletion, and because the characteristic time for establishment of Henry's Law equilibrium is short relative to the time interval required for homogenization of entrained air parcels, our assumption appears to be justified.

Systematic differences exist between the sets of $\overline{E/E^*_{filt}}$ and $\overline{K}_p$ values from the airborne studies conducted in 1991 and 1992. This result, shown in Figures 7a-7b, is attributed to the unintentional sampling of solute H_2O_2 released from droplets that impact and freeze on the forward-facing surface of the air sample inlet. This interpretation is consistent with our previous observations of inefficient H_2O_2 retention during riming [*Snider et al.*, 1992a] and with calculations (see section 2.1) which indicate that increasing the inlet diameter leads to a larger mass of intercepted cloud water. An evaluation of the dominant systematic errors leads us to conclude that our 1991 measurements of $\overline{K}_p$ are in agreement with the temperature-extrapolated laboratory measurements. Furthermore, the large negative departures between the 1992 $\overline{K}_p$ values and the extrapolated laboratory measurements is consistent with the fact that the inlet used in 1992 had a substantially larger cross section than that used in 1991.

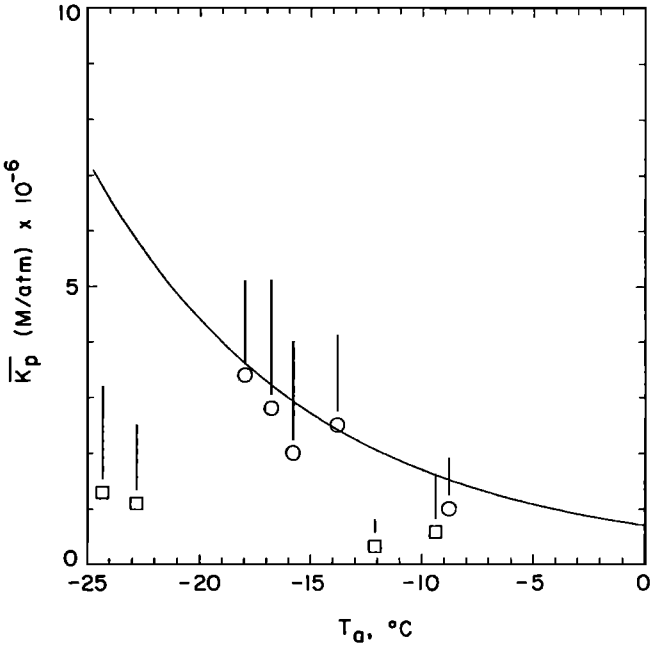

Figure 7b. Cloud-pass averaged Henry's law constants, derived using measurements conducted in 1991 (open circles) and 1992 (open squares), plotted versus the cloud-pass-averaged temperature. Values of LWC from the FSSP probe were used these calculations. The upper limit error bars were calculated using the technique discussed in the text. Values of K, calculated using (3), are also illustrated.

If our interpretation is correct, the experiments conducted during 1991 afford the first validation, conducted in supercooled natural clouds, of the validity of extrapolations of K. This validation is significant, since increasing H_2O_2 solubility with decreasing temperature compensates for the fact that the $S(IV)/H_2O_2$ reaction rate constant decreases with decreasing temperature. As a consequence, predictions of the importance of hydrogen peroxide-mediated sulfate production in clouds characterized by droplet pH values less than 4.5 are also reinforced. Furthermore, this work points to a significant bias that results due to droplet accretion and the concomitant inefficient trapping of dissolved solute that can occur during sampling in supercooled clouds.

Acknowledgments. Assistance provided by the staff of the Department of Atmospheric Science is greatly appreciated. This work was supported by National Science Foundation grants ATM-9012805 and ATM-9314358.

References

Barth, M. C., D. A. Hegg, P. V. Hobbs, J. G. Walega, G. L. Kok, B. G. Heikes, and A. L. Lazrus, Measurements of atmospheric gas-phase and aqueous-phase hydrogen peroxide concentrations in winter on the east coast of the United States, *Tellus*, *41B*, 61-69, 1989.

Claiborn, C. S., and V. P. Aneja, Measurements of atmospheric hydrogen peroxide in the gas phase and in cloud water at Mt. Mitchell, North Carolina, *J. Geophys. Res.*, *96*, 18,771-18,787, 1991.

Conklin, M. H., A. Sigg, A. Neftel, R. C. Bales, Atmosphere-snow transfer function for H_2O_2: Microphysical considerations, *J. Geophys. Res.*, *98*, 18,367-18,376, 1993.

Cooper, W. A., W. R. Sand, M. K. Politovich, and D. L. Veal, Effects of icing on performance of a research airplane, *J. Aircr.*, *21*, 708-715, 1984.

Cooper, W. A., and G. Vali, The origin of ice in mountain cap clouds, *J. Atmos. Sci.*, *38*, 1244-1259, 1981.

Detwiler, A., N. C. Knight, and A. J. Heymsfield, Measurement of liquid/solid mass loading in clouds, in Preprint Volume of the 1990 Conference on Cloud Physics, pp. 318-323, Am. Meteorol. Soc., Boston, Mass., 1990.

Davis, C. I., The ice-nucleating characteristics of various AgI aerosols, Ph.D. dissertation, pp. 267, Univ. of Wyo., Laramie, 1974.

Faust, B., C. Anastasio, J. M. Allen, T. Arakaki, Aqueous-phase photochemical formation of peroxides in authentic cloud and fog waters, *Science*, *260*, 73-75, 1993.

Gallagher, M. W., et al., Case studies of the oxidation of sulfur dioxide in a hill cap cloud using ground and aircraft based measurements, *J. Geophys. Res.*, *95*, 18,517-18,537, 1990.

Gordon, G. L., and J. D. Marwitz, An airborne comparison of three PMS probes, *J. Atmos. Oceanic Technol.*, *1*, 22-27, 1984.

Gunz, D. W., and M. R. Hoffmann, Atmospheric chemistry of peroxides: A review, *Atmos. Environ.*, *24A*, 1601-1633, 1990.

Heikes, B. G., G. L. Kok, J. G. Walega, and A. L. Lazrus, H_2O_2, O_3 and SO_2 measurements in the lower troposphere over the eastern United States during fall, *J. Geophys. Res.*, *92*, 915-931, 1987.

Hidy, G. M., *Atmospheric Sulfur and Nitrogen Oxides*, p. 44, Academic, San Diego, Calif., 1994.

Huang, J., Measurements of O_2 and H_2O_2 retention in rime ice, pp. 64, M.S. thesis, Univ. of Wyo., Laramie, 1994.

Jacob, D., Comment on "The photochemistry of a remote stratiform cloud" by William L. Chameides, *J. Geophys. Res.*, *90*, 5864, 1985.

Jacob, P., and D. Klockow, Measurements of hydrogen peroxide in Antarctic ambient air, snow and firn cores, *Fresenius J. Anal. Chem.*, *346*, 429-434, 1993.

Jaenicke, R., Tropospheric Aerosols, in *Aerosol-Cloud-Climate Interactions*, edited by P.V. Hobbs, Academic, San Diego, Calif., 1993.

Langmuir, I., and K. B. Blodgett, Mathematical investigation of water-droplet trajectories, *U.S. Air Force Tech. Rep. 5418*, U.S. Army Air Forces, 1946.

Lazrus, A. L., G. L. Kok, J. A. Lind, S. N. Gitlin, B. G. Heikes, and R. Shetter, Automated fluorometric method for hydrogen peroxide in air, *Anal. Chem.*, *58*, 594-597, 1986.

Lind, J. A., and G. L. Kok, Henry's law determination for aqueous solutions of hydrogen peroxide, methylhydroperoxide, and peroxyacetic acid, *J. Geophys. Res.*, *91*, 7889-7895, 1986.

Lind, J. A., and G. L. Kok, Correction to "Henry's law determination for aqueous solutions of hydrogen peroxide, methylhydroperoxide, and peroxyacetic acid" by John A. Lind and Gregory L. Kok, *J. Geophys. Res.*, *99*, 21119-21119, 1994.

Locatelli, J. D., and P. V. Hobbs, Fall speeds and masses of solid precipitation particles, *J. Geophys. Res.*, *79*, 2185-2197, 1974.

Lozowski, E. P., J. R. Stallabrass, and P. F. Hearty, The icing of an unheated, nonrotating cylinder, I, A simulation model, *J. Clim. Appl. Meteor.*, *22*, 2053-2062, 1983.

Macdonald, A. M., K. G. Anlauf, C. M. Banic, W. R. Leaitch, and H. A. Wiebe, Airborne measurements of aqueous and gaseous hydrogen peroxide during spring and summer in Ontario, Canada, *J. Geophys. Res.*, *100*, 7253-7262, 1995.

Murphy, T. M., Airborne measurements of hydrogen peroxide partitioning within supercooled clouds, pp. 75, M.S. thesis, Univ. of Wyo., Laramie, 1993.

Nicholls, S., The dynamics of stratocumulus: Aircraft observations and comparisons with a mixed layer model, *Q.J.R. Meteorol. Soc.*, *110*, 783-820, 1984.

Noone, K. J., J. A. Ogren, K. B. Noone, A. Hallberg, S. Fuzzi, and J. A. Lind, Measurements of the partitioning of hydrogen peroxide in a stratiform cloud, *Tellus*, *43B*, 280-290, 1991.

Penkett, S. A., B. M. R. Jones, K. A. Brice, and A. E. J. Eggleton, The importance of atmospheric ozone and hydrogen peroxide in oxidizing sulfur dioxide in cloud and rain water, *Atmos. Environ.*, *13*, 123-137, 1979.

Politovich, M. K., and G. Vali., Observations of liquid water in orographic clouds over Elk Mountain, *J. Atmos. Sci.*, *40*, 1300-1312, 1983.

Politovich, M. K., and W. A. Cooper, Variability of the supersaturation in cumulus clouds, *J. Atmos. Sci.*, *45*, 1651-1664, 1988.

Pruppacher, H. R., and J. D. Klett, *Microphysics of Clouds and Precipitation*, D. Reidel, Norwell, Mass., 1980.

Ridley, B. A., Recent measurements of the oxidized nitrogen compounds in the troposphere, *Atmos. Environ.*, *25A*, 1905-1926, 1991.

Schonbaum, G. R., and B. Chance, Catalase, *The Enzymes*, edited by P. D. Boyer, vol. *13*, pp. 363-408, Academic, San Diego, Calif., 1976.

Snider, J. R., D. C. Montague, and G. Vali, Hydrogen peroxide retention in rime ice, *J. Geophys. Res.*, *97*, 7569-7578, 1992a.

Snider, J. R., D. C. Montague, and T. Murphy, Airborne and mountain-summit observations of H_2O_2 in air parcels identified by the release of SF_6, *EOS Trans. AGU*, *73*, (14), Spring Meet. Suppl., 88-89, 1992b.

Staffelbach, T. A., and G. L. Kok, Henry's law constants for aqueous solutions of hydrogen peroxide and hydroxymethyl hydroperoxide, *J. Geophys. Res.*, *98*, 12,713-12,717, 1993.

Twohy, C. H., and D. Rogers, Airflow and water-drop trajectories at instrument sampling points around the Beechcraft King Air and Lockheed Electra, *J. Atmos. Oceanic Technol.*, *10*, 566-578, 1993.

Vincent, J. H., D. C. Stevens, D. Mark, M. Marshall, and T.

A. Smith, On the aspiration characteristics of large-diameter, thin-walled aerosol sampling probes at yaw orientations with respect to the wind, *J. Aerosol Sci.*, *17*, 211-224, 1986.

Wagman, D. D., W. H.Evans, V. B.Parker, R. H.Schumm, I. Halow, S. M. Bailey, K. L. Churney, and R. L. Nuttall, The NBS tables of chemical thermodynamic properties; Selected values for inorganic and C1 C2 organic substances in SI units, *J. Phys. Chem. Ref. Data*, Suppl., 11, 2, 1982.

T. Murphy and J. R. Snider, University of Wyoming, Department of Atmospheric Science, P.O. Box 3038, Laramie, WY 82071-3038. (e-mail: snider@grizzly.uwyo.edu)

(Received February 3, 1995; revised June 14, 1995; accepted June 16, 1995.)